ADVANCED MATERIALS TECHNOLOGIES
www.advmattechnol.de

Ink Formulation for Printed Organic Electronics: Investigating Effects of Aggregation on Structure and Rheology of Functional Inks Based on Conjugated Polymers in Mixed Solvents

Stefan Schlisske, Christine Rosenauer, Tobias Rödlmeier, Kai Giringer, Jasper J. Michels, Kurt Kremer, Uli Lemmer, Svenja Morsbach, Kostas Ch. Daoulas,* and Gerardo Hernandez-Sosa*

The utilization of solution-processable organic semiconducting (OSC) polymers and the development of industrial-relevant printing techniques enable cost-efficient fabrication of optoelectronic devices for the mass market. Yet, the adaptation of viscoelastic properties of a functional ink to the respective printing technology is challenging. One crucial parameter is the formulation of the ink, which can be adjusted by selecting the combination of solvents that are mixed with the OSC. The current study considers model functional inks composed of a poly-phenylene-vinylene-based OSC and two solvents, empirically known to be good. Their quality is quantified using the Hansen solubility parameters. The influence of the composition of the solvent mixture on structural, dynamical, and rheological behavior of the ink is investigated with light scattering, viscometry, and rheometry. Although both solvents are considered good, polymer aggregation is found at all compositions. Aggregation depends on composition in a nontrivial way. For dilute and semi-dilute inks, the effects of aggregates on the ink viscosity are hidden by the difference in viscosities of the neat solvents. For elevated concentrations, the aggregates produce a hysteresis in the shear-dependent viscosity, which should be considered when developing a functional ink for a particular printing technique.

1. Introduction

The development of organic semiconductors (OSCs) opens opportunities for fabricating optoelectronic devices such as solar cells, organic light-emitting diodes (OLEDs), organic field-effect transistors or organic photodetectors via solution processing.[1–4] Especially the utilization of industrially established printing and coating techniques such as inkjet, gravure, flexo- or screen-printing or slot-die coating has gained significant research interest. These techniques enable high-throughput and cost-efficient fabrication of devices, as well as new applications in the fields of health care, "internet-of-things", or communication.[5–8] Currently, substantial improvement in the performance of printed devices has been achieved by simultaneously addressing material and processing aspects.[9–11] Despite this progress, a deeper understanding of the effects of ink formulation, drying behavior, and the printing technique itself is necessary to defeat still existing challenges, related to the loss of device performance when translating and upscaling laboratory results to industrial scale.

In contrast to "conventional" printing, where pattern and color reproduction are important,[12] printed films in organic electronics must retain the (opto-) electronic functionality intended by the chemical design of the OSC. Here, a key challenge is that the (opto-) electronic properties of the printed films are significantly affected by their morphology, which stems from a complex interplay between various phenomena occurring during delivery and positioning of functional inks on the substrates, as well as their solidification, i.e. "drying". Therefore, obtaining device elements with reasonable performance is a complex optimization problem of numerous ink and process-related

S. Schlisske, Dr. T. Rödlmeier, K. Giringer, Prof. U. Lemmer, Dr. G. Hernandez-Sosa
Light Technology Institute
Karlsruhe Institute of Technology
Engesserstrasse 13, Karlsruhe 76131, Germany

The ORCID identification number(s) for the author(s) of this article can be found under https://doi.org/10.1002/admt.202000335.

DOI: 10.1002/admt.202000335

S. Schlisske, Dr. T. Rödlmeier, K. Giringer, Prof. K. Kremer, Dr. K. Ch. Daoulas, Dr. G. Hernandez-Sosa
InnovationLab
Speyerer Strasse 4, Heidelberg 69115, Germany

C. Rosenauer, Dr. J. J. Michels, Prof. K. Kremer, Dr. S. Morsbach, Dr. K. Ch. Daoulas
Max Planck Institute for Polymer Research
Ackermannweg 10, Mainz 55128, Germany
E-mail: morsbachs@mpip-mainz.mpg.de; daoulas@mpip-mainz.mpg.de

Prof. U. Lemmer
Institute of Microstructure Technology
Karlsruhe Institute of Technology
Hermann-von-Helmholtz-Platz 1, Eggenstein-Leopoldshafen 76344, Germany

parameters, such as viscosity, surface tension, wetting, volatility, and drying rates.[13–15]

Selecting the ink formulation is one of the crucial parts of the optimization procedure. Typically, the inks used in organic electronics are multicomponent polymer solutions—mixtures where the polymeric OSC is dissolved in a combination of solvents. While the conjugated backbones of the OSC polymers provide the (opto-) electronic functionalities, their high molecular stiffness and strong π–π-interactions make them essentially insoluble in any solvent. The flexible side chains attached to the conjugated backbone aim to mitigate this problem. Nevertheless, even with such tailored molecular architectures, conjugated polymers can only be dissolved in specific sets of solvents. Commonly, the use of a binary system of "good" solvents has been the means of choice for fabricating functional devices with homogeneous layer topography.[14,16] Combining two solvents is motivated by empirical observations that adding a second solvent influences surface tension and drying time. Moreover, it enables the adjustment of viscoelastic properties towards the rheological window of the chosen printing technique.[16,17] The control over the aforementioned parameters is crucial for alleviating undesired effects such as coffee-stain formation or viscous fingering, which are detrimental to the film topography and device functionality.[18,19]

Yet, the theoretical prediction of the viscosity of multicomponent solutions of OSC polymers is not straightforward and, therefore, the adjustment of their rheological properties usually requires multiple trial-and-error iterations.[20–22] In a printing experiment, the quality of a solvent is typically rated by optical inspection without taking into account the underlying molecular picture. That is, the solvent is considered "good" if no residuals of the polymer can be observed at the target concentration, necessary to obtain a certain viscosity. In a microscopic view, various studies[19,23–28] conclude that the polymeric OSC in their solvated state show a significantly more complex behavior compared to the standard textbook case of polymers in good solvent conditions.[29,30] OSC polymers tend to form clusters and aggregates, even in solvents that are nominally considered as good. Currently, the understanding of the molecular structure of aggregates and mechanisms underlying their formation is limited. For aromatic solvents, theoretical studies have suggested that aggregates can be stabilized through polymer–solvent complexation via π–π-interactions but the role of the side chains remains unclear.[31,32] Whereas the theoretical understanding of aggregation phenomena is still under development, experimental findings clearly demonstrate that manipulating the aggregated state through solvent choice based on semi-empirical arguments is a promising method for controlling the properties of the ink and the functionality of the final printed device.[24,27,28]

In this work, we explore the effects of aggregation on one of the most crucial properties of functional inks—their viscosity. Surprisingly, so far, the effects of aggregation on the viscoelastic behavior of solutions of OSC polymers have been investigated only in a few studies.[24,25,27] To the best of our knowledge, such studies have only considered solutions of OSC polymers in a single solvent. Spectroscopic measurements were used to demonstrate polymer aggregation; however, such experiments can provide only limited information concerning the structure of the aggregates itself.

Here, we manage to directly quantify the size of the aggregates and systematically correlate aggregation behavior with viscosity benefiting from a special choice of ink components. Our model systems are representative of actual functional inks, being composed of a poly(*p*-phenylene vinylene) (PPV)-based polymer (PDY-132; colloquially known as "Super Yellow" (SY), see **Figure 1**a) that is widely used as an emitter material for OLEDs and the fully miscible solvents toluene and methyl benzoate. This binary solvent system is selected from a range of solvents that are standard for printed electronics but, at the same time, allow for structural characterization of the dissolved polymer component with light scattering experiments. The structural, dynamical, and rheological properties of our model

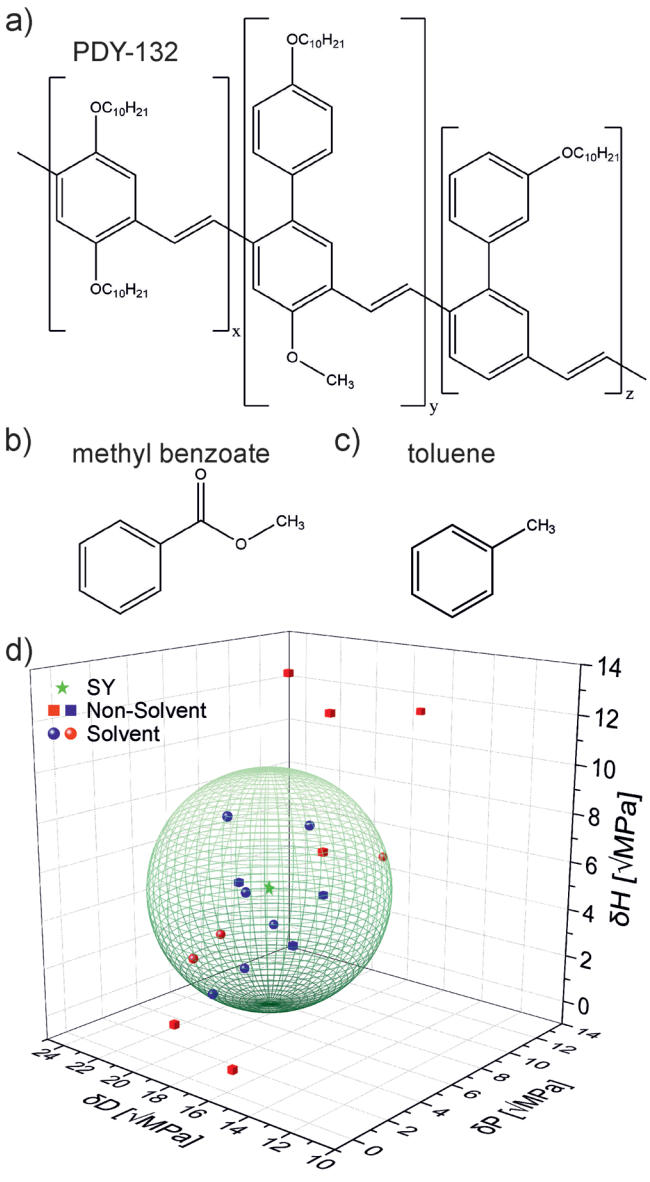

Figure 1. Molecular structure of a) SY according to Gambino et al.,[40] b) methyl benzoate, and c) toluene. d) Solubility sphere of SY and the respective solvents used to determine the HSP; cubes represent non-solvents and dots solvents; blue objects are located inside the sphere and red objects outside the sphere.

inks are quantified for polymer concentrations ranging from the dilute up to the concentrated regime. The measurements cover the entire range of possible mole ratios of the two solvents. The dynamical and rheological behavior is investigated with rolling-ball viscometry and shear rheometry. To understand the observed trends, we estimate the solubility of the OSC polymer in the different solvents through a qualitative analysis based on Hansen solubility parameters (HSP). In the dilute and weakly semi-dilute regimes, we find that the average amount of polymer chains in an aggregate is the smallest for those binary solvent systems where the solubility of the polymer is the highest. The solubility is adjusted by mixing the two solvents at different ratios. We demonstrate that the interpretation of the behavior of the viscosity of dilute inks, as a function of their formulation, requires the combined consideration of aggregation and viscosity of the neat solvent mixture. At elevated polymer concentrations, our measurements indicate that the formation of large aggregates may correlate with memory effects observed in the viscoelastic properties of the functional ink.

2. Results and Discussion

2.1. Solubility Parameters

The SY is mixed with two fully miscible solvents toluene and methyl benzoate (see Figure 1). Before quantifying structural, dynamical, and rheological properties of SY-based solutions, we estimate the affinity of toluene and methyl benzoate towards the polymer via the HSP. The HSP approach is a method based on the Hildebrand and Scott solubility model describing the attractive forces between molecules through the cohesive energy density.[33] This model can be used to select or predict a collection of solvents that can dissolve a certain material, e.g., to determine orthogonal solvents for the solution deposition of dielectrics on semiconducting materials.[34] In the original approach of Hildebrand and Scott, the cohesive energy density of substances is quantified through a single solubility parameter $\delta = \sqrt{E/V_m}$, where E and V_m are the energy of vaporization and molar volume, respectively.[33] In the more elaborate HSP model, the dispersive, polar, and H-bonding contributions to molecular interactions are considered in a distinct way and are assigned separate contributions: δ_D, δ_P, and δ_H.[35] Using the HSP model, all materials can be placed in a 3D coordinate system where the axes represent δ_D, δ_P, and δ_H.

For polymers/solvents with known HSP, the affinity between the polymer (p) and the solvent (s) is quantified via their "distance" R_A in the aforementioned coordinate system, as described by Equation (1), where the subscript specifies the respective substance.[35] In principle, the smaller the distance R_A, the better the compatibility between solvent and polymer

$$(R_A)^2 = 4\left(\delta_{D,p} - \delta_{D,s}\right)^2 + \left(\delta_{P,p} - \delta_{P,s}\right)^2 + \left(\delta_{H,p} - \delta_{H,s}\right)^2 \quad (1)$$

In contrast to most solvents, the HSP for polymers are usually unknown. The parameters of the latter are determined from their solubility in solvents with known HSP. First, the solubility of the polymer for a given nominal concentration in each solvent is qualitatively rated as "good" (i.e., soluble) or "bad" (i.e., non-soluble), following the criteria explained in the Experimental Section and the Supporting Information. By fitting a sphere into the coordinate system covering most of the good solvents and excluding the non-solvents, a polymer-specific solubility sphere with "solubility radius" R_0 is obtained. The center of the sphere represents the coordinates of the polymer in HSP space.

We determined the HSP of SY by following this procedure with the help of the commercial HSPiP software.[36] The used solvents, as well as their HSP alongside with the qualitative analysis of the solubility of SY, are displayed in Table S1, Supporting Information. **Table 1** lists the obtained HSP of SY, as well as those for toluene and methyl benzoate.[35] For comparison, the table reproduces[37] the HSP for poly[2-methoxy-5-(2-ethylhexyloxy)-1,4-phenylenevinylene] (MEH-PPV) and poly[2-methoxy-5-(3,7-dimethyloctyloxy)-1,4-phenylenevinylene (MDMO-PPV), i.e., two other luminescent polymers of the PPV family. The HSP of these polymers were determined at similar concentrations as for SY. Interestingly, the HSP of MEH-PPV and MDMO-PPV are almost identical, whereas the dispersive and polar contributions to the HSP of SY differ by 5–10% from their counterparts in MEH-PPV and MDMO-PPV. The systematically lower values of δ_D and δ_P in SY might stem from the specific molecular architecture of SY, see Figure 1, which has been purposefully engineered to promote disorder and avoid close packing of chain backbones.[38]

Figure 1d displays the solubility sphere of SY as a green wireframe with the HSP of SY in its center, marked as a green star. The solvents used to determine the HSP are displayed as cubes if they do not dissolve the polymer and circles if SY is dissolved. Their respective colors refer to their position inside (blue) or outside the solubility sphere (red). The solubility sphere provides a guideline for predicting solvents, capable of dissolving the polymer. Nevertheless, besides the uncertainty associated with the qualitative nature of the assessment of polymer solubility, even the HSP reported for solvents themselves are subject to significant spread. With this respect, methyl benzoate itself is an illustrative example, for which both $\delta_D = 18.9$ √MPa[35] and $\delta_D = 17.0$ √MPa[39] has been reported. Hence, if R_A is smaller than R_0, it is likely that the considered solvent dissolves the polymer; in the opposite case, it might be a bad solvent or non-solvent. The solvents found inside the solubility region $R_A < R_0$ can be further rated according to the magnitude of R_A: the larger the R_A the lower the quality of the solvent.

Table 2 lists the solubility radii for SY, MEH-PPV, and MDMO-PPV, as well as the R_A values for toluene and methyl benzoate, as calculated using Equation (1). Interestingly, despite the fact that SY has been engineered to exhibit enhanced solubility, its solubility radius is smaller than for the other two PPV derivatives. This apparent discrepancy might originate

Table 1. HSP of polymers and solvents.

Material	δ_D [√MPa]	δ_P [√MPa]	δ_H [√MPa]
Super Yellow	18.0	4.7	5.5
MEH-PPV[37]	19.1	5.4	5.4
MDMO-PPV[37]	19.1	5.6	5.3
Toluene	18.0	1.4	2.0
Methyl benzoate	18.9	8.2	4.7

Table 2. Radius of the solubility sphere of the polymers R_0 and the corresponding R_A.

	Super Yellow	MEH-PPV	MDMO-PPV
R_0 [√MPa]	4.8	6.0	5.5
R_A toluene [√MPa]	4.8	5.7	5.7
R_A methyl benzoate [√MPa]	4.0	2.9	2.7

from different experimental conditions used to determine the HSP of the molecules, the set of solvents, and the qualitative assessment of the solubility itself. Besides, HSP are affected by the molecular weight and the nominal concentration of the polymer. The molecular weight and the polydispersity of the PPV derivatives used by Duong et al.[37] are unknown, so it is not clear to what extent these molecular parameters are similar to those of our SY polymer.

The comparison of R_A reveals that toluene is a marginal solvent for all three polymers since in all cases $R_A \approx R_0$ (bearing, of course, in mind the abovementioned uncertainties). In contrast, for all PPV derivatives, the R_A for methyl benzoate is consistently, and significantly, smaller than R_0. In other words, the HSP model predicts that methyl benzoate accommodates all polymers well. To identify the origins of the higher affinity of methyl benzoate towards MEH-PPV and MDMO-PPV than SY, we compare the dispersive, polar, and H-bonding contributions to R_A^2 (see Equation (1)). To serve as a measure of the incompatibility between the PPV derivative and methyl benzoate along the dispersive, polar, and H-bonding axis of solubility space, the contributions are normalized by R_0^2 of the considered polymer. The calculated contributions are listed in Table S2, Supporting Information, and demonstrate that for all three polymers the discrepancy is strongest along the polar direction, with the highest value encountered for SY. On the phenomenological level of HSPs, we conclude therefore that the higher affinity of methyl benzoate towards MEH-PPV and MDMO-PPV, in comparison to SY, stems mostly from closer agreement of the polar component.

2.2. Dilute Regime

We explore the effect of formulation on structural, dynamical, and rheological properties of SY-based solutions by first considering mixtures with low polymer concentration. **Figure 2**a presents the gyration radius, R_g, and the hydrodynamic radius, R_h, measured in SY solutions using static and dynamic light scattering (LS), respectively, as a function of toluene volume fraction $\phi_{toluene}$. In all these measurements, the SY concentration was fixed to 0.1 g L^{-1} and all samples were filtered through 0.45 µm pore size filters. Interestingly, both R_g and R_h change with $\phi_{toluene}$ nonmonotonously, presenting a minimum at $\phi_{toluene} \approx 10\%$. Because SLS and DLS are independent experiments, the qualitative similarities between the dependencies of R_g and R_h on $\phi_{toluene}$ serve as an important cross-check of the accuracy of our LS measurements. The nonmonotonous variation of the size of the scattering objects observed in Figure 2a allows for two interpretations: 1) our scattering objects are isolated chains whose average conformations respond to the composition of the solvent mixture or 2) our scattering objects

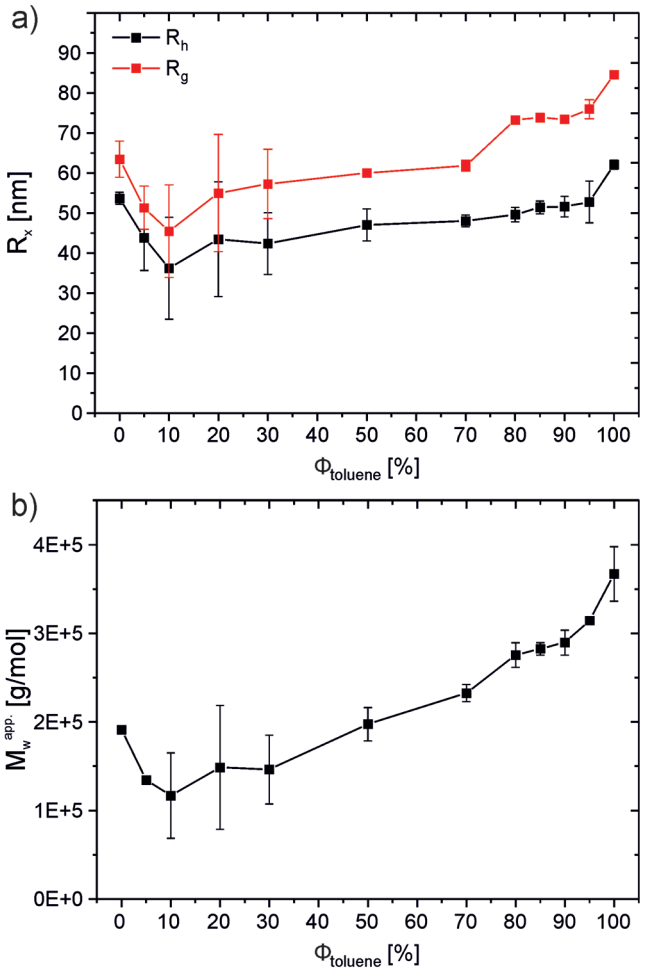

Figure 2. a) Dependence of hydrodynamic radius R_h (black) and gyration radius R_g (red) of SY on toluene volume fraction ϕ measured by LS in toluene/methyl benzoate solutions. b) Apparent mass M_w^{app} of scattering objects in toluene/methyl benzoate solutions at different ϕ.

rather are aggregates of SY chains and the amount of clustered polymers is affected by the composition of the solvent mixture.

In case of the first scenario, the curve in Figure 2a would be consistent with the intriguing phenomenon of co-nonsolvency, where polymers form globules in dilute mixtures with two good solvents.[41–50] For co-nonsolvency, it is essential that both solvents dissolve the polymer but one of them—termed cosolvent—has a much stronger affinity for the polymer, and that the fraction of cosolvent is small. The preference of cosolvent molecules for the polymer, in combination with their tiny amount, promotes the simultaneous binding of cosolvent with two or more repeating units belonging to the same chain. Thus conformational loops are formed, initiating the collapse of the chain into a globule. However, at large concentrations of cosolvent, repeating units can bind with multiple cosolvent molecules. Entropically costly loops are avoided and the chain remains swollen. Therefore, in mixtures following the co-nonsolvency scenario the size of the chains changes nonmonotonously with cosolvent concentration,[30,50] akin to Figure 2a.

A strong argument against the co-nonsolvency scenario comes from the qualitative HSP analysis (cf. Table 2), which

suggests that the solubility of SY in toluene is lower than in methyl benzoate. Therefore, the reduced size of scattering objects at small concentrations $\phi_{toluene} \approx 10\%$ cannot be explained by toluene acting as cosolvent. To unequivocally rule out the co-non-solvency scenario and demonstrate that the scattering objects in Figure 2a are not isolated chains, we quantify their apparent molecular weight M_w^{app} as a function of $\phi_{toluene}$ in Figure 2b. The plot demonstrates that the M_w^{app} is not constant but changes nonmonotonously with solvent composition. Therefore, the scattering objects in Figure 2a are in fact not isolated chains but small aggregates. Unfortunately, we cannot precisely quantify the number of polymer chains in SY clusters because of uncertainties related to the molecular weight of the SY. For instance, gel permeation chromatography (GPC) based on a poly(paraphenylene) (PPP) calibration delivers $M_n \approx 164\,000$ g mol^{-1} and $M_w \approx 390\,000$ g mol^{-1} for our SY. The M_w^{app} in Figure 2b are smaller than these values obtained by GPC. The reason is that the determination of the absolute values of M_w via GPC and static LS relies on different assumptions and theoretical considerations. The M_w in GPC is extracted relative to a known PPP standard and is determined in tetrahydrofuran (THF), i.e., in a solvent other than toluene and methyl benzoate. Complete elution and no loss by filtration are assumed. In static LS the determination of M_w relies on the extrapolation of the refractive index increment, $\delta_n\ \delta_c^{-1}$, from literature values available for PPV. Hence, it is not possible to estimate the amount of clustered chains, e.g., as the ratio $M_w^{app}\ M_w^{-1}$. However, the quantification of relative changes reported in Figure 2b is reliable, since the analysis of all static LS experiments relies on the same assumptions. We emphasize that the determination of R_h and R_g does not depend on the estimated $\delta_n\ \delta_c^{-1}$. Therefore, the plots in Figure 2a,b are independent from each other and it can be safely concluded that the detected change in the size of scattering objects, as a function of $\phi_{toluene}$, stems from the change in the amount of clustered polymers. We are, therefore, convinced that our SY solutions follow the second scenario.

We remind that the gyration radius of a scattering object, quantified by R_g is defined as the root-mean-square distance of the parts of the object from its center of mass. In contrast, R_h quantifies its hydrodynamic radius, meaning the radius of an equivalent sphere that has the same diffusion coefficient as the scattering object. In principle, the parameter $\rho = R_g\ R_h^{-1}$ provides information about the shape and the structure of scattering objects.[51] In our study, however, we cannot extract meaningful information on the aggregates in this way. The reason is that ρ is influenced by several factors, such as the object's aspect ratio and polydispersity in size. Hence objects with qualitatively different structure can, in principle, produce the same ρ. A proper interpretation of this parameter requires additional structural information from complementary techniques.

The observation that SY forms small aggregates in toluene and methyl benzoate, even though on a "macroscopic level" both solvents dissolve SY, agrees with previous findings.[24,26] For example, Wang et al. considered the dilution of MEH-PPV in toluene, chloroform, and 1,2-dichlorobenzene.[26] Small aggregates of MEH-PPV have been observed in all three solvents, irrespective of whether their HSP coordinates are located inside or near the surface of the solubility sphere. Remarkably, the strongest aggregation was reported for 1,2-dichlorobenzene,[26] although the analysis of single-chain conformations at ultra-low polymer concentrations indicated that the solvent quality of 1,2-dichlorobenzene for MEH-PPV is the highest (comparing to the other two solvents). Thus, these observations highlight the importance of a more fundamental analysis and understanding of the effects of ink formulation, beyond empirical macroscopic definitions of solubility.

In our case, some of the features characterizing the dependence of the size of the aggregates on the composition of the solution are consistent with the simple HSP analysis. Specifically, the observation that the largest aggregates are formed in solutions with $\phi_{toluene} = 100\%$ toluene and that their size reduces when methyl benzoate is added agrees with the HSP estimate that methyl benzoate is a better solvent than toluene. However, quite surprisingly, Figure 2a,b suggest that the smallest aggregates might be obtained not at 100% of methyl benzoate ($\phi_{toluene} = 0\%$) but when methyl benzoate is mixed with 5–10% toluene. On the one hand, this nonmonotonous behavior should be approached with some caution because of the statistical noise of the data, which is maximized for concentrations 10–30% toluene, i.e., in the vicinity of the minimum. On the other hand, the increase of the statistical noise in this region can be also seen as an additional indication of a non-trivial solubility behavior. Moreover, earlier studies also suggest that the solubility of conjugated polymers in mixtures of certain solvents may have a nonmonotonous dependence on composition.[52] Intriguingly, the increased solubility at 10–30% toluene suggested by Figure 2a,b is reminiscent of a co-solvency phenomenon, where polymers swell in mixtures of two poor solvents.[30,53]

The filtration of the samples during their preparation for the LS measurements, "preconditions" (cf. Section 2.3) the dilute ink by breaking, at least, the largest aggregates. Therefore, an interesting question is whether the trends in aggregation, summarized in Figure 2, would remain unchanged after long periods of sample storage. In this work, we did not perform additional LS measurements after a week or a month. In practice, however, the sample queuing for the LS device varied the timeframe between sample preparation and completion of LS measurements—from half a day to 2 days. We can confirm that, for such variations, no changes in aggregation trends were observed in individual samples across several series of LS experiments. We speculate that one or two days would be sufficient for observing changes in LS, if the nanoscale aggregates had a strong tendency to agglomerate into larger entities. Indeed, we can roughly estimate the characteristic time τ it takes an aggregate to diffuse a length scale comparable with its own size R_g, from the Einstein relation $R_g^2 = 6D\tau$. The diffusion coefficient of the aggregates is known from LS and is about $D \approx 10^{-12}$ m^2 s^{-1}. Substituting $R_g^2 \approx 10^{-15}$ m^2 (cf. Figure 2a) yields $\tau \approx 10^{-4}$ s only. Whereas no LS measurements were conducted after long-term storage, we have confirmed through visual inspection that no macroscopic aggregation occurred in samples that were kept at 20 °C for several weeks.

To quantify the effects of aggregation on viscosity, we performed rheological measurements in the dilute regime using a rolling-ball viscometer. We take into account that the viscosity of a polymer solution can be phenomenologically expanded with respect to the polymer mass concentration c as[29,54]

$$\eta(\phi) = \eta_s(\phi) + \eta_s(\phi)\left[\eta(\phi)\right]c + k_H(\phi)\eta_s(\phi)\left(\left[\eta(\phi)\right]c\right)^2 \quad (2)$$

In this expression, $\eta_S(\phi)$ is the viscosity of mixed solvents without the polymer, $[\eta(\phi)]$ is the intrinsic viscosity, and $k_H(\phi)$ is the Huggins coefficient. The explicit argument ϕ indicates that these quantities depend on the composition of the solvent mixture. Equation (2) is not restricted to well-dissolved chains only, but is also applicable when aggregates are formed.[54]

Considering Equation (2), we present the dependence of $\eta(\phi) - \eta_S(\phi)$ on $\phi_{toluene}$ for several concentrations of SY (solid symbols) in **Figure 3**a. For reference, Figure 3a also presents the viscosity of the solvents and their mixtures $\eta_S(\phi)$ (dashed line). For representative samples, we measured the viscosity several times and observed that the variation between these measurements is small. A more essential contribution to the statistical noise of the data, "jaggedness" of the curves, stems from variations during sample preparation and is harder to estimate. Therefore, we provide no error bars in Figure 3a. From the plots in Figure 3a, we can quantify the overlap concentration c^* of the SY solutions, considering that, phenomenologically, c^* is often taken as the concentration at which the polymer solution is about two times as viscous as the pure solvent.[54] The plots in Figure 3a demonstrate that $\eta(\phi) \approx 2\eta_S(\phi)$ when $c = 0.7$–1 g L^{-1}, which means that the SY solutions for $c \lesssim 1$ g L^{-1} are found in the dilute or weakly semi-dilute regime.

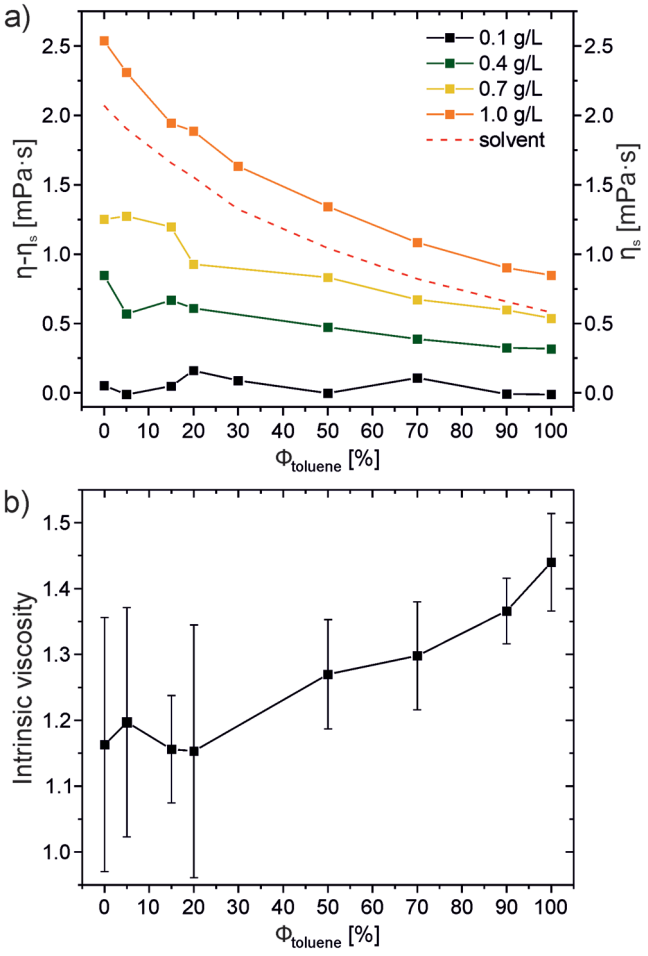

Figure 3. a) Dependence of η-η_s on toluene volume fraction, ϕ, for different concentrations of SY (reported in the labels). Here, η and η_s are, respectively, the viscosities of the solution and the mixture of pure solvents. The viscosity of mixtures of pure solvents—without polymer—is shown separately by the orange line. b) Dependence of the intrinsic viscosity $[\eta]$ on ϕ.

Because our solutions are found in the dilute or weakly semi-dilute regime, we fit $\eta(\phi)$ at each $\phi_{toluene}$ as a function of c, retaining only the linear term in Equation (2). We employ a standard least squares linear fit[55] and present the extracted intrinsic viscosity $[\eta(\phi)]$ in Figure 3b. Because we are lacking an estimate of the experimental error σ with which the source data $\eta(\phi)$ are determined, we calculate the error bars of $[\eta(\phi)]$ using a standard method[55] based on the estimate $\sigma^2 = \chi^2 (N-2)^{-1}$. Here, χ^2 is the sum of the squared residuals of the least-squares line and $N = 4$ is the number of different polymer concentrations that were considered ($c = 0$, 0.4, 0.7, and 1 g L^{-1}) for the fit. The plot demonstrates that polymer aggregation increases the intrinsic viscosity. The highest $[\eta(\phi)]$ is found in pure toluene ($\phi_{toluene} = 100\%$) where the largest aggregates are observed. Adding methyl benzoate decreases $[\eta(\phi)]$; a trend which is consistent with the reduction of aggregation. Overall, the dependence of $[\eta]$ on ϕ is monotonous and we cannot conclude, within the accuracy of our data, whether there is any minimum of $[\eta(\phi)]$ near $\phi_{toluene} = 10\%$.

Interestingly, in our mixtures, the effects of SY aggregation on the viscosity $\eta(\phi)$ are hidden by the trends characterizing the viscosity of the neat solvent mixture, i.e., without the polymer. Because methyl benzoate is almost four times more viscous than toluene (cf. dashed line in Figure 3a), the highest viscosities in dilute inks of SY are observed in mixtures that are rich in methyl benzoate, even though in this case the SY shows the weakest aggregation. In other words, we observe in Figure 3a that the dependence of $\eta(\phi) - \eta_S(\phi)$ on $\phi_{toluene}$ follows a trend opposite to $[\eta(\phi)]$. In solutions where $\eta_S(\phi)$ depends only weakly on $\phi_{toluene}$, we expect that the changes in $[\eta(\phi)]$ caused by aggregation will have an explicit footprint on the dependence of viscosity on composition $\eta(\phi)$.

2.3. Elevated Concentrations

The results of the previous section demonstrate that, for the functional inks considered in this work, the correlations between polymer aggregation and viscosity in the dilute regime are not directly discernible. For printing processes, however, most relevant are semi-dilute and concentrated solutions, motivating us to address also the regime of elevated polymer concentrations. Since inks can experience shear rates ranging over several orders of magnitude, depending on the selected printing or coating technique or even within different stages of the same process, it is relevant to investigate their shear behavior.[56,57] Therefore, we performed shear-dependent viscosity measurements of SY solutions with various solvent ratios at concentrations relevant for printing processing of optoelectronic devices.[9,15,57] Furthermore, we investigated the hysteresis using a sequence of four shear sweeps in order to determine a possible influence of the aggregation on the magnitude of the fluid viscosity.

Figure 4a reports the relative viscosity $\eta\ \eta_S^{-1}$ as a function of the shear rate, $\dot{\gamma}$, for an ink containing 8.5 g L^{-1} of SY at three

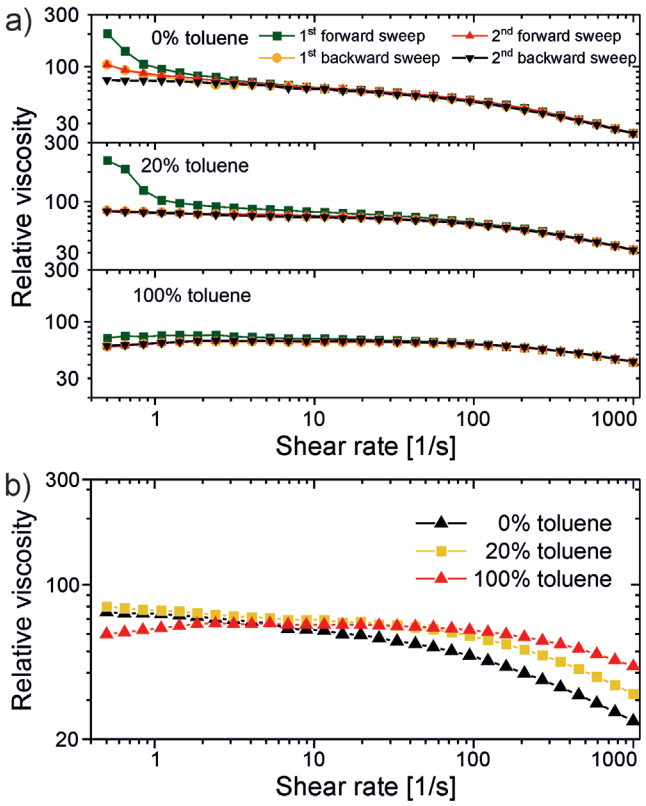

Figure 4. a) Sweep-dependent measurement of relative viscosity $\eta\ \eta_s^{-1}$ of SY solutions in pure methyl benzoate (top); 80:20 methyl benzoate:toluene (middle) and pure toluene (bottom) as a function of shear rate, $\dot{\gamma}$. b) Dependence of the relative viscosity $\eta\ \eta_s^{-1}$ of SY solutions on shear rate, $\dot{\gamma}$. The three cases correspond, respectively, to solutions in pure methyl benzoate (black) 80:20 methyl benzoate:toluene (yellow) and pure toluene (red) measured in the second forward sweep.

different volume fractions of toluene: $\phi_{toluene}$ = 0%, 20%, and 100%. For all considered $\phi_{toluene}$, the viscosity of the ink exhibits shear-thinning behavior and is smaller in the first "backward" sweep (orange circles) than in the first "forward" rheological measurement (green squares). For the 100% and 20% toluene samples, this "rheological hysteresis" vanishes during the second "forward" (red triangles) and the second "backward" (black triangles) sweeps, where the dependencies of $\eta\ \eta_S^{-1}$ on $\dot{\gamma}$ follow closely each other. For the 0% toluene sample, however, the hysteresis is somewhat more protracted: there is still some difference in the viscosities at low shear rates between the second "forward" and "backward" sweeps. For this composition, the viscosity presents its lowest value only after the second "backward" sweep, where it reaches the same order of magnitude as the other two solvent ratios. Interestingly, along the first sweep, the SY solutions that are rich in methyl benzoate are more viscous, in terms of the relative viscosity $\eta\ \eta_S^{-1}$, than the toluene-rich mixtures. The situation reverses along the second forward and backward rheological measurements, where toluene-rich mixtures show weaker shear-thinning and have larger $\eta\ \eta_S^{-1}$. This effect is especially prominent at higher shear rates, whereas at low shear rates, the solution might still be affected by large polymer agglomerates. To illustrate the effect more clearly, Figure 4b presents a collective plot of $\eta\ \eta_S^{-1}$ measured along the final backward "branch" for the three cases of $\phi_{toluene}$. For these experiments, the examined solutions were prepared 24 h prior to use and were stirred at 50 °C and cooled down to room temperature without stirring prior to being measured. A plausible explanation of our rheological observations is that the kinetics of SY dilution at high concentrations is a very slow process. It cannot be significantly accelerated by stirring, where mechanical perturbations are rather weak. The kinetics seems to be slower in methyl benzoate than in toluene. The first shear deformation acts as a stronger mechanical influence that promotes the dilution further. After the hysteresis is eliminated, the rheology is determined rather by the "equilibrium-like" aggregation. According to Figures 2 and 3, the propensity for aggregation is stronger in toluene than in methyl benzoate, which explains why the toluene-rich solutions show the highest relative viscosity during the last "hysteresis-free" branch of the rheological measurements.

Strong dependencies of viscosity on shear history, as those documented in Figure 4a,b, can be critical for successful printing of homogeneous layers. For instance, if the polymer aggregation induced by the solvent composition influences the viscosity behavior of the ink during the printing process, it could affect the formation of drops in inkjet printing or cell filling in gravure printing.[13,17,58] Of course, the influence of the very high shear rates associated with inkjet printing (>10^6 s^{-1}) is outside the scope of the present experiment. Nevertheless, the observed aggregation can have an influence on the characteristics of the deposited layer and ultimately on the optoelectronic properties of the device and should therefore be considered when designing a functional ink.[19,24,28,59]

3. Conclusions

We investigated ternary solutions of a standard PPV-based conjugated polymer, SY, in mixtures of methyl benzoate and toluene. These solutions are an example of functional inks used in printed electronics for fabricating device elements, such as active layers of OLED. Structural, dynamical, and rheological properties were investigated for a broad range of SY concentrations and ratios of the two solvents, using complementary experimental techniques including dynamic and static light scattering (DLS/SLS), rolling-ball viscometry, and shear rheometry. HSP were estimated for SY to facilitate qualitative miscibility analysis. The main messages of our study for industrial application of multicomponent functional inks in printed electronics can be summarized as follows.

First, our LS experiments highlighted the limitations of macroscopic, empirical characterizations of solubility. Such phenomenological characterizations are common when developing solubility models, such as HSP, for coatings and printing industry. Specifically, we found that nanoscale aggregation (clustering) of polymer chains occurs in all studied solutions of SY, even though both methyl benzoate and toluene are empirically known to dissolve SY on macroscopic scales. This result is consistent with previous studies reporting small-scale aggregation of PPV-based polymers in a broad range of nominally "good" solvents.[24,26] A plausible explanation is that the kinetics of nanoscale dilution of conjugated polymers is a very

slow process, which favors long-lived clusters comprising a few polymer chains. For the preparation of our samples, we used a standard protocol based on micro-filtration, which cannot mitigate nanoscale aggregation. This suggests that the determination of solubility parameters in conjugated polymers might benefit from including an ultrafiltration step.

Second, the viscosity of the ink is significantly affected by the viscosity of the solvent medium, at least in the dilute and the semi-dilute concentration regimes. The polymer component contributes only a weaker "perturbation." For the inks studied here, aggregation correlates directly only with the intrinsic viscosity of the polymer: the largest intrinsic viscosity was observed in toluene-rich solutions where the largest aggregates were formed. However, the largest values of the actual viscosity were obtained in methyl benzoate-rich solutions. This apparent discrepancy is simply the consequence of the fact that methyl benzoate is substantially more viscous than toluene. In mixtures containing solvents with similar viscosity, the footprint of aggregation on the composition-dependent properties of the fluid is expected to be more prominent. Because the viscosities of the solvents play a dominant role, they must be considered explicitly when engineering the rheological behavior of the ink.

Third, polymer aggregation in a functional ink, prior to printing, can be substantial. Large aggregates at elevated polymer concentrations may be one of the factors that cause a strong dependency of rheological properties on the "history" of the ink. We observed that at elevated concentrations, a reproducible shear-thinning curve could be obtained only after the ink was preconditioned with back and forth shear deformations. Presumably, these deformations facilitated the breaking of large polymer aggregates and promoted the mixing of SY with the solvents. Therefore, we suggest that an optimum ink formulation protocol should include an ink precondition step that avoids effects induced by aggregation in multi-solvent ink systems. Such step should be tailored to the printing technique being utilized and have a positive influence on the final optoelectronic properties of the printed film.

4. Experimental Section

Determination of HSP: The HSP for the commercially available polymer PDY-132 ("SY," Merck) were determined by evaluating the solubility of the material in a variety of solvents. For this, 1.0–2.0 mg of SY was weighed in a 1.5 mL vial and mixed with the appropriate amount of solvent to reach a concentration of 2.5 g L^{-1}. The vials were placed on a laboratory shaker for 24 h at room temperature prior to the evaluation of the solubility. For each solution, the solubility was qualitatively rated with a value of "1" if the polymer was dissolved or "0" if the polymer was not dissolved. This distinction was made by evaluating the homogeneity of the solution against a white back light. If any remaining solid was visible in the solution, the polymer was considered "not dissolved" and the respective solvent was rated with "0." Conversely, if no residuals were visible, the polymer was considered "dissolved" and the solvent was rated with "1." This set of data (Table S1, Supporting Information) was then fed into the HSPiP software developed by Hansen, Abbot, and Yamamoto, which calculates the solubility sphere with an iterative algorithm. The HSP were extracted after the third iteration.

Dynamic and Static Light Scattering: The DLS/SLS experiments were conducted on a commercially available instrument from ALV GmbH consisting of an electronically controlled goniometer and an ALV-5004 multiple tau full-digital correlator (320 channels). As a light source, a HeNe laser with a wavelength of 632.8 nm and an output power of 25 mW (JDS Uniphase, Type 1145P) was utilized. For the measurements, SY was dissolved at a concentration of 1 g L^{-1} in pure toluene and pure methyl benzoate. All other samples were then prepared by dilution to 0.1 g L^{-1} and mixing the appropriate ratios of the stock solutions. All sample solutions were filtered through Millex-LCR 0.45 µm filters (Merck Millipore) directly into quartz light scattering cuvettes (inner diameter 18 mm), which were cleaned before with distilled acetone in a Thurmond apparatus to remove dust. The light scattering measurements were then performed at a constant temperature of 20 °C. With DLS, the z-average diffusion coefficients were determined after angular-dependent measurements and extrapolated to $q \rightarrow 0$. The hydrodynamic radius was then calculated via the Stokes–Einstein equation. From SLS measurements, the radius of gyration was determined via a Zimm linearization from the slope of the scattering curve. The refractive index increment $\delta_n\ \delta_c^{-1}$ used for the calculation of the apparent molecular weights was determined by interpolation from the values for pure toluene and methyl benzoate. For toluene, a $\delta_n\ \delta_c^{-1}$ of 0.314 L g^{-1} was assumed according to the literature value reported for a poly(phenylenevinylene) derivative from Li et al.[60] Additionally, the $\delta_n\ \delta_c^{-1}$ for methyl benzoate was extrapolated from the literature values for toluene and chloroform and determined to be 0.338 g L^{-1}.

Determination of the Molecular Weight: For relative molecular weight determination of SY, a PSS SECcurity Agilent 1260 Infinity Setup (Polymer Standards Service GmbH (PSS)) was used, including a column from PSS (SDV 10^6, 10^4, 500 Å, 300 × 8 mm) maintained at 30 °C and a PSS SECcurity UV detector. The eluent was THF with a flow rate of 1 mL min^{-1}. The UV detector signal was used at a wavelength of 254 nm and the relative molecular weights were calculated based on a universal PPP calibration. The sample was injected at a concentration of 0.1 g L^{-1} in THF after filtration through 0.45 µm Millex-LCR filters.

Viscosity Determination: For the determination of viscosities in dilute conditions, samples with concentrations of 0.1, 0.4, and 0.7 g L^{-1} were prepared from the original 1 g L^{-1} solution for toluene, methyl benzoate, and the solvent mixtures. Then, for each solution, the density was measured using a DM40 density meter (METTLER-TOLEDO GmbH) and the kinematic viscosity using a Lovis 2000 M rolling-ball microviscometer (Anton Paar Germany GmbH). The dynamic viscosity was then calculated from the density and kinematic viscosity for each sample. All measurements were performed at 20 °C.

Rheometry: Shear rheometry was performed for SY dissolved in toluene (EMSURE, Merck) and methyl benzoate (Merck, EMPLURA) and a mixture of both with a concentrations of 8.5 g L^{-1}.The solvents were filtered with a 0.45 µm polyvinylidene fluoride filter prior to use. The solutions were stirred at 50 °C for 24 h prior to the viscosity measurements. All the steps were performed in ambient cleanroom conditions. The rheometry measurements were done with a rotational rheometer with cone/plate geometry (HAAKE MARS, Thermo Scientific).

Supporting Information

Supporting Information is available from the Wiley Online Library or from the author.

Acknowledgements

The authors thank Kaloian Koynov for fruitful discussions and proofreading of the manuscript. The authors thank the Institute of Printing, Science and Technology (IDD) of the TU Darmstadt for their support in determining the HSP for SY. The authors acknowledge the financial support from the German Federal Ministry for Education and Research (BMBF) through the grants FKZ 13N13691 and FKZ 13N13694.

Conflict of Interest

The authors declare no conflict of interest.

Keywords

ink formulation, light scattering, polymer aggregation, printed electronics, viscosities

Received: April 9, 2020
Revised: May 14, 2020
Published online:

[1] Y. Cui, Y. Wang, J. Bergqvist, H. Yao, Y. Xu, B. Gao, C. Yang, S. Zhang, O. Inganäs, F. Gao, J. Hou, *Nat. Energy* **2019**, *4*, 768.
[2] M. Pietsch, T. Rödlmeier, S. Schlisske, J. Zimmermann, C. Romero-Nieto, G. Hernandez-Sosa, *J. Mater. Chem. C* **2019**, *7*, 7121.
[3] W. J. Scheideler, R. Kumar, A. R. Zeumault, V. Subramanian, *Adv. Funct. Mater.* **2017**, *27*, 1606062.
[4] K. Tsai, M. Hung, Y. Mao, S. Chen, *Adv. Funct. Mater.* **2019**, *29*, 1901025.
[5] L. Inzelberg, M. David Pur, S. Schlisske, T. Rödlmeier, O. Granoviter, D. Rand, S. Steinberg, G. Hernandez-Sosa, Y. Hanein, *Flexible Printed Electron.* **2018**, *3*, 045001.
[6] M. Mayer, A. J. Baeumner, *Chem. Rev.* **2019**, *119*, 7996.
[7] C. Vega-Colado, B. Arredondo, J. Torres, E. López-Fraguas, R. Vergaz, D. Martín-Martín, G. del Pozo, B. Romero, P. Apilo, X. Quintana, M. A. Geday, C. de Dios, J. Sánchez-Pena, *Sensors* **2018**, *18*, 3045.
[8] D. Corzo, K. Almasabi, E. Bihar, S. Macphee, D. Rosas-Villalva, N. Gasparini, S. Inal, D. Baran, *Adv. Mater. Technol.* **2019**, *4*, 1900040.
[9] L. Merklein, D. Daume, F. Braig, S. Schlisske, T. Rödlmeier, M. Mink, D. Kourkoulos, B. Ulber, M. Di Biase, K. Meerholz, G. Hernandez-Sosa, U. Lemmer, H. Sauer, E. Dörsam, P. Scharfer, W. Schabel, *Colloids Interfaces* **2019**, *3*, 32.
[10] F. Mathies, H. Eggers, B. S. Richards, G. Hernandez-Sosa, U. Lemmer, U. W. Paetzold, *ACS Appl. Energy Mater.* **2018**, *1*, 1834.
[11] N. Strobel, M. Seiberlich, R. Eckstein, U. Lemmer, G. Hernandez-Sosa, *Flexible Printed Electron.* **2019**, *4*, 043001.
[12] M. Rosen, N. Ohta, *Color Desktop Printer Technology*, CRC Press, Boca Raton, FL **2006**.
[13] G. Grau, J. Cen, H. Kang, R. Kitsomboonloha, W. J. Scheideler, V. Subramanian, *Flexible Printed Electron.* **2016**, *1*, 023002.
[14] S. Magdassi, *The Chemistry of Inkjet Inks*, World Scientific, Singapore **2009**.
[15] B. Derby, *Annu. Rev. Mater. Res.* **2010**, *40*, 395.
[16] G. Hernandez-Sosa, N. Bornemann, I. Ringle, M. Agari, E. Dörsam, N. Mechau, U. Lemmer, *Adv. Funct. Mater.* **2013**, *23*, 3164.
[17] S. Calvi, F. Maita, M. Rapisarda, G. Fortunato, A. Valletta, V. Preziosi, A. Cassinese, L. Mariucci, *Org. Electron.* **2018**, *61*, 104.
[18] C. McDowell, M. Abdelsamie, M. F. Toney, G. C. Bazan, *Adv. Mater.* **2018**, *30*, 1707114.
[19] F.-C. Chen, H.-C. Tseng, C.-J. Ko, *Appl. Phys. Lett.* **2008**, *92*, 103316.
[20] Y. Marcus, *Solvent Mixtures: Properties and Selective Solvation*, Taylor and Francis, London **2002**.
[21] L. T. Novak, *Ind. Eng. Chem. Res.* **2003**, *42*, 1824.
[22] A. Dondos, D. Patterson, *J. Polym. Sci., Part A-2: Polym. Phys.* **1969**, *7*, 209.
[23] T. Q. Nguyen, V. Doan, B. J. Schwartz, *J. Chem. Phys.* **1999**, *110*, 4068.
[24] E. Tekin, E. Holder, D. Kozodaev, U. S. Schubert, *Adv. Funct. Mater.* **2007**, *17*, 277.
[25] C. C. Hua, C. L. Chen, C. W. Chang, C. K. Lee, S. A. Chen, *J. Rheol.* **2005**, *49*, 641.
[26] D. Wang, Y. Yuan, Y. Mardiyati, C. Bubeck, K. Koynov, *Macromolecules* **2013**, *46*, 6217.
[27] H. Hu, K. Zhao, N. Fernandes, P. Boufflet, J. H. Bannock, L. Yu, J. C. De Mello, N. Stingelin, M. Heeney, E. P. Giannelis, A. Amassian, *J. Mater. Chem. C* **2015**, *3*, 7394.
[28] M. S. Chen, O. P. Lee, J. R. Niskala, A. T. Yiu, C. J. Tassone, K. Schmidt, P. M. Beaujuge, S. S. Onishi, M. F. Toney, A. Zettl, J. M. J. Fréchet, *J. Am. Chem. Soc.* **2013**, *135*, 19229.
[29] M. Rubinstein, R. H. Colby, *Polymers Physics*, Oxford University Press, Oxford **2003**.
[30] D. Mukherji, C. M. Marques, K. Kremer, *Annu. Rev. Condens. Matter Phys.* **2020**, *11*, 271.
[31] M. H. Rahman, S. C. Liao, H. L. Chen, J. H. Chen, V. A. Ivanov, P. P. J. Chu, S. A. Chen, *Langmuir* **2009**, *25*, 1667.
[32] N. E. Jackson, K. L. Kohlstedt, B. M. Savoie, M. Olvera De La Cruz, G. C. Schatz, L. X. Chen, M. A. Ratner, *J. Am. Chem. Soc.* **2015**, *137*, 6254.
[33] J. H. Hildebrand, R. L. Scott, *The Solubility of Nonelectrolytes*, Reinhold Publishing Corporation, New York **1950**.
[34] A. M. Gaikwad, Y. Khan, A. E. Ostfeld, S. Pandya, S. Abraham, A. C. Arias, *Org. Electron.* **2016**, *30*, 18.
[35] C. M. Hansen, *Hansen Solubility Parameters: A User's Handbook*, CRC Press, Boca Raton, FL **2007**.
[36] S. Abbott, C. M. Hansen, H. Yamamoto, R. S. Valpey, *Hansen Solubility Parameters in Practice*, Hansen-Solubility.com, Denmark **2015**.
[37] D. T. Duong, B. Walker, J. Lin, C. Kim, J. Love, B. Purushothaman, J. E. Anthony, T.-Q. Nguyen, *J. Polym. Sci., Part B: Polym. Phys.* **2012**, *50*, 1405.
[38] H. Spreitzer, H. Becker, E. Kluge, W. Kreuder, H. Schenk, R. Demandt, H. Schoo, *Adv. Mater.* **1998**, *10*, 1340.
[39] C. M. Hansen, *Hansen Solubility Parameters: A User's Handbook*, CRC Press, Boca Raton, FL **2000**.
[40] S. Gambino, A. K. Bansal, I. D. W. Samuel, *Org. Electron.* **2010**, *11*, 467.
[41] H. G. Schild, M. Muthukumar, D. A. Tirrell, *Macromolecules* **1991**, *24*, 948.
[42] F. M. Winnik, H. Ringsdorf, J. Venzmer, *Macromolecules* **1990**, *23*, 2415.
[43] H. Kojima, F. Tanaka, C. Scherzinger, W. Richtering, *J. Polym. Sci., Part B: Polym. Phys.* **2013**, *51*, 1100.
[44] C. Wu, X. Wang, *Phys. Rev. Lett.* **1998**, *80*, 4092.
[45] J. Walter, J. Sehrt, J. Vrabec, H. Hasse, *J. Phys. Chem. B* **2012**, *116*, 5251.
[46] S. Backes, P. Krause, W. Tabaka, M. U. Witt, D. Mukherji, K. Kremer, R. Von Klitzing, *ACS Macro Lett.* **2017**, *6*, 1042.
[47] K. Kyriakos, M. Philipp, C. H. Lin, M. Dyakonova, N. Vishnevetskaya, I. Grillo, A. Zaccone, A. Miasnikova, A. Laschewsky, P. Müller-Buschbaum, C. M. Papadakis, *Macromol. Rapid Commun.* **2016**, *37*, 420.
[48] C. Dalgicdir, F. Rodríguez-Ropero, N. F. A. Van Der Vegt, *J. Phys. Chem. B* **2017**, *121*, 7741.
[49] J. J. Magda, G. H. Fredrickson, R. G. Larson, E. Helfand, *Macromolecules* **1988**, *21*, 726.
[50] D. Mukherji, C. M. Marques, K. Kremer, *Nat. Commun.* **2014**, *5*, 4882.
[51] W. Burchard, *Adv. Polym. Sci.* **1983**, *48*, 1.
[52] C. K. Lee, C. C. Hua, S. A. Chen, *Macromolecules* **2011**, *44*, 320.
[53] D. Mukherji, C. M. Marques, T. Stuehn, K. Kremer, *Nat. Commun.* **2017**, *8*, 1374.

[54] I. Teraoka, *Polymer Solutions: An Introduction to Physical Properties*, Wiley, New York **2002**.
[55] W. H. Press, S. A. Teukolsky, W. T. Vetterling, B. P. Flannery, in *Numerical Recipes in C: The Art of Scientific Computing*, (Ed: W. T. Vetterling), Cambridge University Press, USA **1992**, pp. 656–706.
[56] H. Kipphan, *Handbuch der Printmedien: Technologien und Produktionsverfahren*, Springer, Berlin **2013**.
[57] G. Nisato, D. Lupo, S. Ganz, *Organic and Printed Electronics: Fundamentals and Applications*, Pan Stanford Publishing, Singapore **2016**.
[58] D. Jang, D. Kim, J. Moon, *Langmuir* **2009**, *25*, 2629.
[59] Y. Shi, J. Liu, Y. Yang, *J. Appl. Phys.* **2000**, *87*, 4254.
[60] Y. C. Li, C. Y. Chen, Y. X. Chang, P. Y. Chuang, J. H. Chen, H. L. Chen, C. S. Hsu, V. A. Ivanov, P. G. Khalatur, S. A. Chen, *Langmuir* **2009**, *25*, 4668.